View metadata, citation and similar papers at core.ac.uk
brought to you by CORE
provided by Elsevier - Publisher Connector

Available online at www.sciencedirect.com
ScienceDirect
Biochimica et Biophysica Acta 1773 (2007) 457–470
Biochimica et Biophysica Acta BBA
www.elsevier.com/locate/bbamcr

Implications on zinc binding to S100A2

Michael Koch [a], Shibani Bhattacharya [b], Torsten Kehl [a], Mario Gimona [c], Milan Vašák [d], Walter Chazin [b], Claus W. Heizmann [e], Peter M.H. Kroneck [a], Günter Fritz [a,*]

[a] Department of Biology, University of Konstanz, Universitätsstrasse 10, Postfach M665, 78457 Konstanz, Germany
[b] Departments of Biochemistry and Chemistry, Center for Structural Biology, Vanderbilt University, Nashville, TN 37232-8725, USA
[c] Institute of Molecular Biology, Department of Cell Biology, Austrian Academy of Sciences, Billrothstrasse 11, A-5020 Salzburg, Austria
[d] Institute of Biochemistry, University of Zürich, Winterthurerstrasse 190, CH-8051 Zürich, Switzerland
[e] Department of Pediatrics, Division of Clinical Chemistry and Biochemistry, University of Zürich, Steinwiesstrasse 75, CH-8032 Zürich, Switzerland

Received 19 September 2006; received in revised form 7 December 2006; accepted 11 December 2006
Available online 19 December 2006

Abstract

Human S100A2 is an EF-hand calcium-binding S100 protein that is localized mainly in the nucleus and functions as tumor suppressor. In addition to Ca^{2+} S100A2 binds Zn^{2+} with a high affinity. Studies have been carried out to investigate whether Zn^{2+} acts as a regulatory ion for S100A2, as in the case of Ca^{2+}. Using the method of competition with the Zn^{2+} chelator 4-(2-pyridylazo)-resorcinol, an apparent K_d of 25 nM has been determined for Zn^{2+} binding to S100A2. The affinity lies close to the range of intracellular free Zn^{2+} concentrations, suggesting that S100A2 is able to bind Zn^{2+} in the nucleus. Two Zn^{2+}-binding sites have been identified using site directed mutagenesis and several spectroscopic techniques with Cd^{2+} and Co^{2+} as probes. In site 1 Zn^{2+} is bound by Cys21 and most likely by His 17. The binding of Zn^{2+} in site 2 induces the formation of a tetramer, whereby the Zn^{2+} is coordinated by Cys2 from each subunit. Remarkably, only binding of Zn^{2+} to site 2 substantially weakens the affinity of S100A2 for Ca^{2+}. Analysis of the individual Ca^{2+}-binding constants revealed that the Ca^{2+} affinity of one EF-hand is decreased about 3-fold, whereas the other EF-hand exhibits a 300-fold decrease in affinity. These findings imply that S100A2 is regulated by both Zn^{2+} and Ca^{2+}, and suggest that Zn^{2+} might deactivate S100A2 by inhibiting response to intracellular Ca^{2+} signals.
© 2006 Elsevier B.V. All rights reserved.

Keywords: S100; S100A2; Zinc; Calcium; Cobalt

1. Introduction

S100 proteins are small acidic EF-hand calcium-binding proteins comprised of a modified, S100-specific EF-hand at the N-terminus and a classical C-terminal EF-hand [1]. All S100 proteins, with the exception of the evolutionarily distinct S100G, form homo- and hetero-dimers. These proteins show remarkable cell- and tissue-specific expression patterns, and are involved in widely different processes including cell cycle regulation, cell growth, differentiation and motility. Dysregulation of specific S100 proteins is associated with a variety of human diseases, including cancer, and neurodegenerative and cardiovascular disorders [2].

Human S100A2 is unique among the S100 proteins because it is predominantly localized in the nucleus [3]. S100A2 was identified as a tumor suppressor in human mammary epithelial cells, and downregulation of the protein was observed in tumor tissues of prostate adenocarcinoma, lung cancer and breast carcinoma [4]. Recent studies show that S100A2 binds and activates p53, in a Ca^{2+}-dependent manner [5]. This finding directly links the tumor suppressing activities of S100A2 and p53 and suggests a positive regulation of p53 through S100A2. So far only the biochemical and regulatory properties of human S100A2, but not from orthologs of other mammals, have been studied to some extent. S100A2 orthologs are reported in chimpanzee (GenBank accession No. XP_513815), dog (GenBank accession No. XP_855158) and cow (GenBank accession No. NM_001034367). The protein from chimpanzee

Abbreviations: ANS, 4,4′-dianilino-1,1′-binaphtyl-5,5′-sulfonic acid; PAR, 4-(2-pyridylazo)-resorcinol

* Corresponding author. Tel.: +49 7531 88 3205; fax: +49 7531 88 2966.
E-mail address: guenter.fritz@uni-konstanz.de (G. Fritz).

0167-4889/$ - see front matter © 2006 Elsevier B.V. All rights reserved.
doi:10.1016/j.bbamcr.2006.12.006

is identical to human S100A2 and contains 4 Cys residues, whereas the orthologs from dog and cow contain only one Cys residue at position 86.

Multi-dimensional NMR studies on S100A2 revealed a molecular architecture similar to that described for other S100 proteins [6]. Each subunit of S100A2 is comprised of four α-helices, [residues 7–21 (helix I), 31–40 (helix II), 52–64 (helix III), and 72–95 (helix IV)] organized into two EF-hands. The protein exhibits an affinity for Ca^{2+} comparable to other S100 proteins, however, it is reported that it binds Zn^{2+} with high affinity [7,8]. Each S100A2 subunit carries four cysteine residues (Cys2, Cys21, Cys86, Cys93) (Fig. 1) that are presumably involved in the coordination of Zn^{2+}. The Zn^{2+}-binding sites of S100A2 have been subject of three investigations, with virtually no consensus as to stoichiometry, affinity, location, and structure. Franz et al. [8] proposed two potential binding motifs including His17–Cys21–His39 and Cys2–Cys86–Cys93, whereas Stradal et al. [7] suggested that two binding sites consist of Cys2–His39 and of His17–Cys86–Cys93. In a study by Randazzo et al. [6], it was concluded that one site is formed by residues His17–Cys21–Cys93 and another by Cys2–His39, with Cys86 participating in either the first or the second binding site. None of these studies included direct measurements of the affinity and stoichiometry of Zn^{2+} bound per S100A2, nor was the possible function of Zn^{2+} binding to S100A2 discussed.

There is emerging evidence for the role of Zn^{2+} as a key regulatory ion in cellular processes [9]. The total Zn^{2+} concentration in eukaryotic cells is on the order of several hundred μM [10], but the majority of intracellular Zn^{2+} is bound to zinc finger proteins [11], metallothioneins [12], and reduced glutathione [13]. The residual free Zn^{2+} concentration is rather low and ranges from pM to nM levels. The concentration of free Zn^{2+} varies in different cell types and changes rapidly upon cellular stimulation. In resting human monocytes and lymphocytes the free Zn^{2+} concentration ranges between 0.17 and 0.35 nM [14]. Similar basal levels are reported for chromaffin cells where the free Zn^{2+} concentration rises from 0.4 to 2 nM upon electrical stimulation [15]. In neurons, the changes in free Zn^{2+} are much more pronounced and show larger amplitudes.

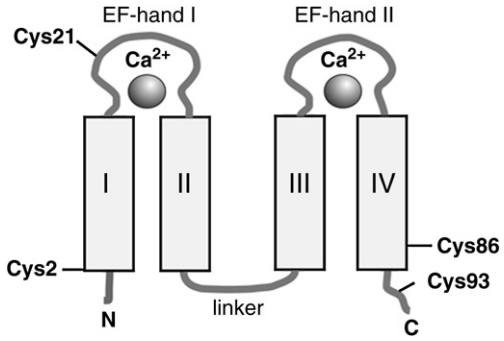

Fig. 1. Location of cysteine residues in a S100A2 subunit. Schematic view a S100A2 subunit based on the structural information by Randazzo et al. [6]. The locations of the four cysteine residues are indicated. Cys2 resides at the N-terminus of helix I, Cys21 in the N-terminal EF-hand, Cys86 at the C-terminus of helix IV, and Cys93 in the unstructured C-terminal region.

Dependent on the type of stimulation and on the extracellular Zn^{2+} concentrations, the free Zn^{2+} levels reach 35–45 nM [16] or even 250–300 nM [17] in cultured neocortical neurons. Within signaling microdomains the transient free Zn^{2+} concentrations have been reported to rise up to 10 μM [18]. The large number of Zn^{2+}-dependent DNA binding and regulatory proteins suggests that changes in free Zn^{2+} are directly translated into altered gene expression [19]. However, there is also an immediate cellular response to elevated Zn^{2+} levels, which activate or inhibit several key enzymes from different signaling cascades [20,21]. Intracellular information transfer by Zn^{2+} binding to proteins, in a manner analogous to Ca^{2+}, was first discussed nearly a decade ago [22]. Interestingly, Zn^{2+} binding to other S100 proteins like S100B or S100A12 increases their affinity for Ca^{2+} affinity [23,24] and directly links Zn^{2+} and Ca^{2+} signaling in the cell.

The potential importance of S100A2 as a nuclear protein linked to p53 prompted studies to determine whether S100A2 binds Zn^{2+} at such low intracellular concentrations and whether Zn^{2+} binding has an effect on the Ca^{2+}-binding properties of S100A2. First, the affinity of S100A2 for Zn^{2+} was quantified. Using site-directed mutagenesis, metal ion-binding studies, spectroscopic methods, and molecular modeling, we demonstrated the existence of two different Zn^{2+}-binding sites. Zn^{2+} binding to site 1 had only minor effects on the protein structure. In contrast, binding of Zn^{2+} in site 2 caused a 300-fold decrease in Ca^{2+} affinity in one EF-hand and the formation of a tetrameric state that has not been observed previously. These results provide a critical foundation for understanding the functional role of Zn^{2+} binding in S100A2.

2. Material and methods

4-(2-pyridylazo)-resorcinol (PAR), 4,4′-dianilino-1,1′-binaphtyl-5,5′-sulfonic acid (bis-ANS), and 2,2′-dithiopyridine were purchased from Fluka. All other reagents were of the highest commercially available grade and were used without further purification.

2.1. Protein expression and purification

Human S100A2 was sub-cloned into the bacterial expression vector pMW172 and cysteine deficient variants were generated by site-directed mutagenesis, as described elsewhere [7]. *E. coli* BL21(DE3) clones expressing the proteins were grown in DYT medium containing 0.2% glucose and 100 μg/ml ampicillin at 310 K. At $OD_{600} \approx 0.6$, 0.5 mM IPTG was added to induce expression. After 3 h the cells were harvested by centrifugation (6,000 g, 20 min) and cell pellets were frozen in liquid nitrogen and stored at 200 K.

To purify the proteins, 10–15 g cells were suspended in 40 ml of 50 mM Tris–HCl (pH 7.6), the solutions were brought to 0.5 mM $MgCl_2$ and 0.4% of PMSF, and a few crystals of DNAse I were added. Cell contents were released by two passages through a French Press at 138 MPa. Then 1 mM EDTA and 5 mM DTT were added and the crude extract was centrifuged at 100,000 g for 1 h. 5 mM $CaCl_2$ was added to the supernatant and loaded onto phenylsepharose column (3.5×10 cm, GE Healthcare) equilibrated with 50 mM Tris–HCl, 5 mM $CaCl_2$, pH 7.6. The column was washed with 1.5 l of the same buffer and S100A2 was eluted with 50 mM Tris–HCl, 10 mM EDTA, pH 7.6. The eluate was concentrated by ultrafiltration (10 kDa, Amicon) and loaded onto a Superdex 75 (2.6×60 cm, GE Healthcare) column equilibrated with 20 mM Tris–HCl, 150 mM NaCl, pH 7.6. Fractions containing S100A2 were combined and concentrated to 10 mg/ml, then stored at 200 K. Purity was controlled by SDS-Page and UV spectra. Protein concentration was calculated using the

specific absorption $\varepsilon_{278\ nm}$=3050±80 M^{-1} cm^{-1} per subunit determined by quantitative amino acid analysis.

Prior to all experiments the proteins were incubated with a 300-fold excess of DTT for 2 h at 310 K to reduce all cysteine residues. Metal ions were removed by addition of 0.5 mM EDTA; both EDTA and DTT were removed on a NAP5 desalting column (GE Healthcare) equilibrated with the chosen buffer.

Human recombinant S100B, which served as a control in several experiments, was prepared as described elsewhere [25].

2.2. Determination of sulfhydryl groups

SH groups were determined with 2,2′-dithiopyridine. Aliquots of the S100A2 variants were added to 6 M Gu–HCl, 10 mM EDTA, 50 mM Tris–HCl, pH 8.3. After mixing, 50 µl of 3.2 mM 2,2′-dithiopyridine in 0.2 M Na–acetate (pH 4.0) was added and the absorption at 343 nm was recorded ($\varepsilon_{343\ nm}$=7,600 M^{-1} cm^{-1}) [26].

2.3. Size exclusion chromatography

A Superdex 75 HR (1.0×30 cm, GE Healthcare) column was calibrated with proteins of known molecular mass. The Zn^{2+}-dependent oligomerisation of the S100A2 proteins was monitored in 20 mM Tris–HCl, 150 mM NaCl, pH 7.6 containing either 100 µM or 1 mM $ZnCl_2$ as running buffers. The concentration of the injected protein was 90 µM (homodimer). $MgCl_2$ was added up to 10 mM to prevent non-specific Zn^{2+} binding to the surface of S100A2.

2.4. Mass spectrometry

Mass spectra were obtained on a PE SCIEX API 365 LC/MS/MS electrospray ionization mass spectrometer (Perkin Elmer). Samples were dialyzed against water and diluted to a final concentration of 50 µg/ml in running medium containing 50% acetonitrile and 0.1% acetic acid or 3 mM ammonium acetate; 20 µl were injected per run.

2.5. Dynamic light scattering

DLS experiments were carried out at 4 °C in the absence or presence of one equivalent of $ZnCl_2$, in quartz micro-cells (1.0 cm) on a DynaPro-MS/X system. Data were analyzed with the program Dynamics (Proterion Corporation).

The concentration of $ZnCl_2$ stock solutions was determined by flame atomic absorption spectrometry (SpectrAA-110, Varian Inc.). The Zn^{2+} content of protein fractions from size exclusion chromatography was determined according to [27] and corrected for the Zn^{2+} concentration of the buffer.

2.6. Determination of Zn^{2+} dissociation constants

The procedure is based on the competition of 4-(2-pyridylazo)-resorcinol ($ZnPAR_2$, K_d=3.0×10^{-13}, 20 mM HEPES–NaOH, pH 7.4) and S100A2 for Zn^{2+} [28]. The protein concentration was 2 µM with PAR at 10 µM in 20 mM HEPES–NaOH, 5 mM $MgCl_2$, pH 7.4. Zn^{2+} was added in 0.5 µM steps. For determinations of Zn^{2+} affinity constants in the presence of Ca^{2+}, 2 mM $CaCl_2$ was added. The assay was carried out at 298 K. It was assumed that the excess of PAR is high enough to form completely a Zn^{2+}–PAR_2 complex. The dissociation constant of Zn^{2+}–PAR_2 was determined photometrically at 494 nm (Eq. 1). The absorption of the Zn^{2+}–PAR_2 complex was measured at different Zn^{2+} concentrations and the dissociation constants of the Zn^{2+}–S100A2 complexes (Eq. 2) were calculated according to Eq. 3.

$$K_d(ZnPAR_2) = \frac{[Zn_{free}]\cdot[PAR_{free}]^2}{[ZnPAR_2]} \quad (1)$$

$$K_d(ZnS100A2) = \frac{[Zn_{free}]\cdot[S100A2_{free}]}{[ZnS100A2]} \quad (2)$$

$$K_d(ZnS100A2) = \frac{K_d(ZnPAR_2)\cdot[ZnPAR_2]\cdot[S100A2_{free}]}{[PAR_{free}]^2\cdot[ZnS100A2]} \quad (3)$$

with $[ZnS100A2]=[Zn^{2+}_{tot}]-[ZnPar_2]$, $[S100A2_{free}]=[S100A2_{tot}]-[ZnS100A2]$, and $[PAR_{free}]=[PAR_{tot}]-2[ZnPar_2]$. $[S100A2]_{tot}$=total concentration of zinc binding sites present in the assay.

2.7. Determination of Ca^{2+} dissociation constants

The Ca^{2+}-binding constants of S100A2 were determined by Ca^{2+} titrations in the presence of the fluorophore chelator BAPTA-5N (Invitrogen) in 10 mM MOPS, 100 mM KCl pH 7.2. The protein concentration was 10 or 20 µM and BAPTA-5N was added to a final concentration of 5 µM. The fluorescence signal of BAPTA-5N was recorded at 522 nm upon excitation at 492 nm and was followed as a function of total Ca^{2+} concentration. The titration curve was analyzed using the program CaLigator [29]. The resulting fits were exported and plotted with the program Origin (OriginLab). BAPTA-based Ca^{2+} indicators are highly selective for Ca^{2+} over Mg^{2+}, however they bind other divalent cations such as Zn^{2+} with much higher affinity. Therefore we assessed the Ca^{2+} affinity in the presence of Zn^{2+} by the Ca^{2+}-dependent change of intrinsic tyrosine fluorescence. The protein concentration in tyrosine fluorescence monitored experiments was 10 µM in 20 mM Tris–HCl, 5 mM $MgCl_2$, pH 7.6. All emission spectra were recorded with a Perkin Elmer LS50B instrument equipped with a thermostatted cell holder at 298 K. Ca^{2+} was titrated to metal-free or to Zn^{2+}-loaded protein until saturation was reached.

2.8. UV/Vis, circular dichroism (CD), and magnetic circular dichroism (MCD)

Solutions of buffers and metal ions (Ca^{2+}, Co^{2+}, Zn^{2+}, Cd^{2+}) were prepared with Chelex 100 (Biorad) treated water throughout. Prior to adjustment of pH, the Chelex 100 resin was added (0.5 g/100 ml) and the solution was stirred for 1 h. After adjustment of pH, the solution was passed through a 0.2 µm filter and stored in metal-free plastic vials. All experiments with Co^{2+} were carried out under exclusion of dioxygen. Dioxygen was removed by 8–10 cycles of vacuum and flushing with argon 5.0; all solutions were stored in a Coy anaerobe chamber (95% N_2/5% H_2) with dioxygen levels below 0.1 ppm.

UV/Vis spectra in the range 280–800 nm were recorded with a Perkin-Elmer Lambda 16 spectrophotometer in 0.1 and 1.0 cm quartz cells. In the case of Zn^{2+} and Cd^{2+}, protein was 30 µM in 20 mM Tris–HCl, 5 mM $MgCl_2$, pH 7.6; for Co^{2+}, protein was 300 µM in 20 mM Tris–HCl, 5 mM $MgCl_2$, pH 8.3. The absorbance was corrected for dilution.

CD and MCD spectra of Co^{2+} complexes were recorded on a Jasco J-810 instrument at a magnetic field of 1.5 T; the differences in extinction ε were calculated according to Nakanishi et al. [30]. UV CD spectra were recorded as described above in 20 mM Tris–HCl, 5 mM $MgCl_2$, pH 7.6, in 0.10 cm and 0.01 cm quartz cells between 180 and 260 nm. The α-helical content was calculated with CDNN 2.1 [31].

2.9. EPR spectroscopy

EPR spectra of Co^{2+}-S100A2 variants in 20 mM Tris–HCl, 5 mM $MgCl_2$, pH 8.3 were recorded on a Bruker Elexsys 500 instrument. Typical experimental conditions were 0.5 mT modulation amplitude, 20 mW microwave power, 9.38 GHz (X-band), and 10 K (ITC 503 temperature control, Oxford Instruments).

2.10. NMR experiments

U-^{13}C,^{15}N labelled S100A2-WT was expressed in *E. coli* grown in minimal media containing $^{13}C_6$-glucose and $^{15}NH_4Cl$ as the sole carbon and nitrogen sources, then purified as described previously [6]. The purified apo-protein was exchanged into a NMR buffer containing 20 mM Tris–HCl, 90% H_2O/10% D_2O at pH 8.0. The buffer was treated with Chelex beads to remove trace metal ions and the dissolved oxygen was removed by bubbling argon through the solution before exchanging the protein into the NMR buffer using NAP5 columns (GE Healthcare). The final protein concentration after the buffer change was determined to be 105 µM, i.e. 52 µM homodimer. Only 0.9 equivalents of Zn^{2+} were added in order to fill only Zn^{2+}-binding site 1 of S100A2. In order to prevent oxidation of the cysteines of S100A2 in the NMR sample (650 µl) the headspace of the NMR tube was purged with argon for 10 min and then sealed gastight. ^{15}N–^{1}H HSQC spectra were acquired on a 600 MHz Bruker AVANCE spectrometer at 300 K.

2.11. Homology modeling

The crystal structures of apo S100A3 (1KSO) [32], apo S100A6 (1K9P), and Ca^{2+}-loaded S100A6 (1K96) [33] served as templates. Modeling was carried out with the programs Modeller [34] and O [35].

3. Results

3.1. Selection and characterization of S100A2 variants

In the previous studies of Zn^{2+} binding to S100A2 it was proposed that cysteine residues play a crucial role. However, it was unclear which of the four cysteine residues (Cys2, Cys21, Cys86, Cys93) per subunit are involved in Zn^{2+} binding. The schematic representation of the two EF-hands within a S100A2 subunit (Fig. 1) shows the location of the 4 cysteine residues. Assuming that one Cys→Ser mutation is sufficient to perturb a Zn^{2+}-binding site effectively, we analyzed the four single mutants. In order to examine the possibility of multiple cysteine-containing zinc sites, two additional S100A2 variants carrying triple Cys→Ser mutations were analyzed.

Wild-type S100A2 and the cysteine variants were expressed and purified to homogeneity. The mutations and the correct size of the proteins were confirmed by mass spectrometry and cysteine analysis (Supplement Table I). Several cysteine residues in S100A2 appeared susceptible to air oxidation as observed previously [7]. Consequently, all manipulations of samples were performed in an atmosphere of 95% N_2 and 5% H_2 to prevent formation of intermolecular or intramolecular disulfide bonds. According to size exclusion chromatography, all of the apo-proteins were homodimers with an apparent mass of about 20 kDa as described for other S100 proteins [4].

The S100A2 variants were examined by CD spectroscopy for possible structural changes induced by the Cys→Ser mutations. The spectra of all variants were closely similar to the spectrum of S100A2-WT. Thus, it is reasonable to assume that the proteins fold to the same structure. Analysis of the secondary structure elements using the program CDNN revealed a content of about 50–55% α-helix for S100A2-WT and all mutants, in good agreement with previous NMR analysis of S100A2 [6]. Moreover, S100A2-WT and all S100A2 variants showed an increase of α-helical content upon the addition of Ca^{2+} (60–65% α-helix), confirming that the Ca^{2+}-induced conformational change occurs in all of the variants.

3.2. Structural characterization of Zn^{2+}-bound S100A2

Zn^{2+} binding to S100A2-WT caused a small but reproducible decrease in the α-helical content of about 3–4% (Fig. 2A, B) as shown by CD spectroscopy. This small conformational change upon Zn^{2+} binding was slightly more pronounced in S100A2-C21S with a decrease of 7% (not shown), but was virtually absent in S100A2-C2S where a decrease of only 0.5–1% was observed (Fig. 2B). Since Zn^{2+} binds via cysteine residues to S100A2 CysS→Zn^{2+} LMCT can overlay the CD signal from the protein backbone and

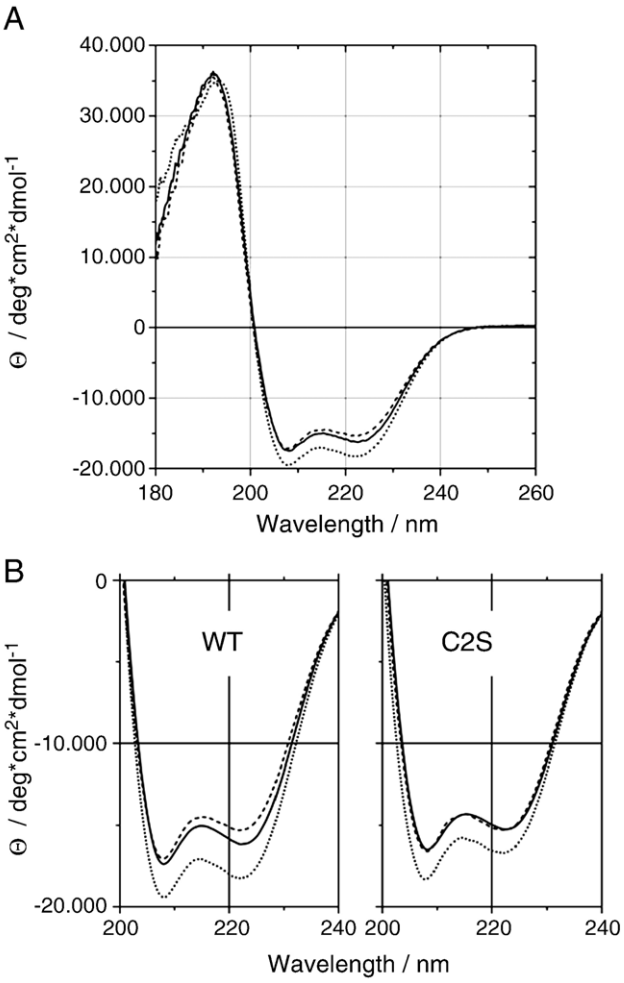

Fig. 2. CD-spectra of S100A2-WT and comparison with S100A2-C2S. Solid line: metal free S100A2, dotted line: Ca^{2+}-loaded S100A2, dashed line: Zn^{2+}-loaded S100A2. (A) CD-spectra of metal free and Ca^{2+}- and Zn^{2+}- loaded S100A2-WT. (B) Comparison of changes in CD upon Zn^{2+} and Ca^{2+} binding to S100A2-WT and S100A2-C2S. The protein concentration was 163 μM with 163 μM Zn^{2+} or with 1.6 mM Ca^{2+} respectively in 20 mM Tris–HCl, pH 7.6.

make the exact quantification of the structural changes difficult.

The influence of Zn^{2+} on the degree of oligomerization of S100A2 and the variants was analyzed by size exclusion chromatography (SEC) and dynamic light scattering. In the absence of Zn^{2+} S100A2-WT and variants eluted from SEC at a volume corresponding to the homodimeric protein. Neither Ca^{2+} nor Mg^{2+} induced major changes in this behavior (data not shown) and no oxidation of Cys residues was observed during the run. However, Zn^{2+}-loaded S100A2-WT and variants which still contain Cys2 eluted at higher apparent molecular mass corresponding to a tetramer (~46 kDa) (Fig. 3). The Zn^{2+}-induced S100A2 tetramer was also observed in the presence of physiological concentrations of Mg^{2+} (0.5 mM). Increasing the Mg^{2+} concentration up to 10 mM did not affect the tetramer formation, showing that the interaction is Zn^{2+} specific. S100A2 variants S100A2–C2S and S100A2–C2S–C86S–C93S lacking Cys2 did not form a tetramer in the presence of

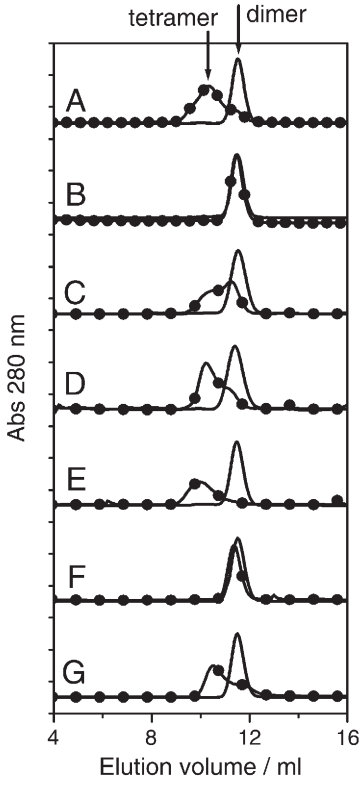

Fig. 3. Zn^{2+}-dependent oligomerization of S100A2-WT and variants monitored by size exclusion chromatography. Superdex 75 HR (1.0×30 cm) column, 20 mM Tris–HCl, pH 7.6, 300 μg protein per run. (A) S100A2-WT, (B) S100A2–C2S, (C) S100A2–C21S, (D) S100A2–C86S, (E) S100A2–C94S, (F) S100A2–C2S–C86S–C93S, and (G) S100A2–C21S–C86S–C93S without Zn^{2+} (solid line) and with 100 μM Zn^{2+} (line and circle). For S100A2–C21S–C86S–C93S 1 mM Zn^{2+} was used.

Zn^{2+} and eluted at the same volume as apo protein. Human recombinant S100B, which also binds Zn^{2+} with high affinity [36] served as a control and did not form larger aggregates in SEC experiments under the same conditions. The formation of the tetrameric species of S100A2-WT upon Zn^{2+} binding was confirmed by dynamic light scattering. As in the size exclusion experiments, S100A2–C2S showed no Zn^{2+}-induced oligomerization and remained dimeric. Thus, only Cys2 is the critical residue responsible for Zn^{2+}-induced S100A2 tetramer formation.

As shown previously [8] by fluorescence experiments using bis-ANS, Ca^{2+} and Zn^{2+} binding to S100A2 induces the exposure of a hydrophobic patch at he surface of the protein. In order to map the Zn^{2+}-binding site that triggers the increase in hydrophobic surface we examined Zn^{2+} dependent bis-ANS binding to S100A2-WT, S100A2–C2S and S100A2–C21S. Whereas S100A2–C21S (site 1 defect, *vide infra*) showed increased bis-ANS fluorescence like S100A2-WT, S100A2–C2S (site 2 defect, *vide infra*) exhibited almost no increase in bis-ANS fluorescence (Supplement Figure III). The results indicate that binding of Zn^{2+} to site 2 but not to site 1 causes the exposure of hydrophobic residues. These data are consistent with an apparent conformational change upon binding of Zn^{2+} to site 2 as monitored by CD spectroscopy (Fig. 2).

3.3. Affinity of S100A2 for zinc

In order to place the binding of Zn^{2+} in an appropriate functional context, the affinity of S100A2 for Zn^{2+} was determined using the competitive chelator PAR (Supplement Figure IV). Other chromogenic or fluorogenic Zn^{2+} chelators such as Zincon or Fluo-Zin3 had been tested but were not suited to determine Zn^{2+}-binding constants of Ca^{2+}-loaded S100A2 because of unspecific interactions of the dyes with the Ca^{2+}-loaded protein. Non-specific Zn^{2+} binding most likely to negatively charged surface residues of S100A2 was observed in initial experiments. These effects were abrogated by the addition of Mg^{2+}, which is present in high concentrations in the cytoplasm, to the solutions. Addition of potassium or sodium salt at the same concentrations did not affect the Zn^{2+} binding. In order to obtain correct affinities, the stoichiometry of Zn^{2+} per S100A2 has to be known. From initial titrations using Zn^{2+}, Cd^{2+}, or Co^{2+} a stoichiometry of about 2.5 Zn^{2+} per S100A2 homodimer was determined. Size exclusion experiments revealed the formation of a tetrameric S100A2 species bridged by Zn^{2+}. Zn^{2+} and Cd^{2+} titrations (*vide infra*) revealed the resulting S100A2 tetramer contains most likely 5 Zn^{2+} per S100A2 tetramer. This value was confirmed by quantitative analysis of the Zn^{2+} content of fractions from size exclusion chromatography containing tetrameric S100A2. The analysis showed that tetrameric S100A2 contained 1.31±0.01 Zn^{2+} per subunit, i.e. 5.2 Zn^{2+} per tetramer. This further dimer–tetramer equilibrium could not be modeled with the present data and made it impossible to extract individual Zn^{2+}-binding constants in S100A2 from the titrations.Therefore in the fits of the Zn^{2+}-binding data we assumed a stoichiometry of 2.5 Zn^{2+} ions per

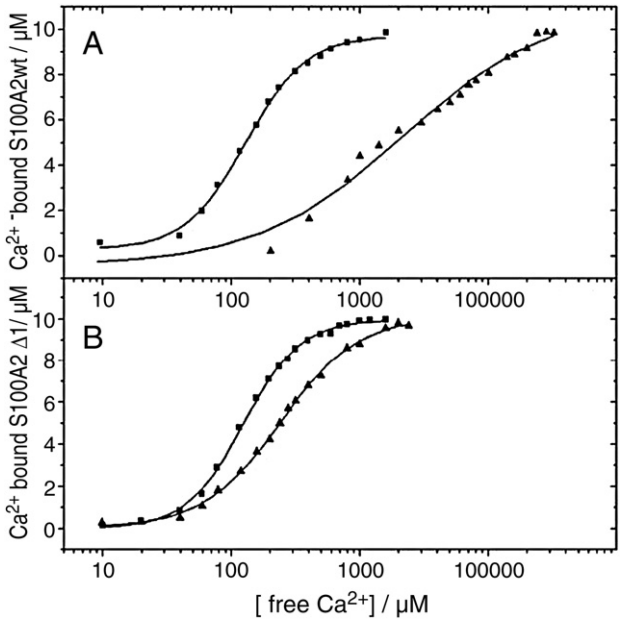

Fig. 4. Binding of Ca^{2+} to S100A2-WT and S100A2-C2S monitored by tyrosine fluorescence. Protein concentration is 10 μM in 20 mM Tris–HCl, 5 mM $MgCl_2$, pH 7.6. (A) binding of Ca^{2+} to S100A2-WT; (B) binding of Ca^{2+} to S100A2–C2S in the absence (■) and presence of 15 μM Zn^{2+} (▲). Ca^{2+}-binding constants are given in Table 2.

Table 1
Apparent dissociation constants of Zn^{2+}– and Co^{2+}–S100A2 complexes

Protein	K_d Zn^{2+}–S100A2 [nM] [a]	K_d Zn^{2+}/Ca^{2+}–S100A2 [nM] [b]	K_d Co^{2+}–S100A2 [μM] [c]
S100A2-WT	25±6 (10)	49±8 (9)	46±1
S100A2–C2S	42±6 (7)	215±30 (7)	49±1
S100A2–C21S	215±70 (9)	600±190 (5)	700±180
S100A2–C86S	22±6 (9)	42±6 (7)	45±8
S100A2–C93S	64±6 (5)	142±30 (5)	470±210
S100A2–C2S–C86S–C93S	245±5 (4)	no binding *	510±60
S100A2–C21S–C86S–C93S	225±150 (4)	no binding *	540±190

[a] Determined with PAR; affinity of apo-S100A2 and Ca^{2+}-loaded S100A2 for Zn^{2+}.
[b] Number of determinations.
[c] Calculated from UV/Vis titrations.
* The affinity was too low to be determined with PAR.

S100A2 homodimer (5 Zn^{2+} ions per S100A2 tetramer) for S100A2-WT and all variants except those that carry a Cys2→Ser2 mutation and do not form the Zn^{2+} dependent tetramer. For these mutants we assumed a stoichiometry of 2 Zn^{2+} ions per S100A2 homodimer.

S100A2-WT binds Zn^{2+} with an apparent K_d=25±6 nM (Table 1). This affinity is about 100-fold higher than previously reported by Franz et al. [8]. The lower affinities reported previously might be due to the fast oxidation of Cys residues in S100A2. In order to determine how different Cys residues contributed to Zn^{2+} binding, the affinity of several Cys→Ser point mutations were determined. Many mutations resulted in decreased affinity for Zn^{2+}. However, none of them abolished Zn^{2+} binding completely (Table 1). A significant effect was observed for S100A2–C21S (K_d=215 nM) and the variants carrying multiple mutations that include C2S, e.g. S100A2–C2S–C86S–C93A (K_d=245 nM). In contrast, S100A2–C86S or S100A2–C93S showed no (K_d=22 nM) or a modest decrease (K_d=64 nM) in Zn^{2+} affinity implying that these residues are not strongly involved in Zn^{2+} coordination. The observed slight reduction in Zn^{2+} affinity of S100A2–C93S was attributed to an allosteric structural effect.

Remarkably, the effects of the Cys→Ser point mutations were much more pronounced for binding of Zn^{2+} to Ca^{2+}-loaded S100A2. While pre-loading with Ca^{2+} decreased the Zn^{2+} affinity of the wild-type protein about 2-fold, Ca^{2+}–S100A2–C21S exhibited a K_d (Zn^{2+}) of 600 nM, i.e. a 12-fold weaker affinity than Ca^{2+}–S100A2–WT. Similarly, Ca^{2+}–S100A2–C2S exhibited a 4-fold lower affinity for Zn^{2+} than Ca^{2+}–S100A2–WT. For Ca^{2+}-loaded S100A2–C2S–C86S–C93S and S100A2–C21S–C86S–C93S mutants, the affinity for Zn^{2+} was too low to be measured by the Zn^{2+} chelator method with PAR. In summary, the two mutations Cys2 and Cys21 had the largest effect on Zn^{2+} affinity. The distance of the two Cys residues in the structure of S100A2 (see Fig. 1) makes it unlikely that both residues are involved in a single binding site. Therefore, we concluded that two distinct Zn^{2+} sites exist: site 1 which employs Cys21 as Zn^{2+} ligand, and site 2 with Cys2 as ligand. Moreover, since the Zn^{2+} affinity towards S100A2 was altered when Ca^{2+} was bound, one can conclude that Ca^{2+} and Zn^{2+} binding to S100A2 are not two independent but rather energetically coupled processes.

3.4. Decrease of calcium affinity by zinc binding

The interplay between Ca^{2+} and Zn^{2+} in S100A2 was further characterized by measurements of the Ca^{2+} affinity of S100A2 in the presence and absence of Zn^{2+}. The binding of Ca^{2+} was followed by intrinsic tyrosine fluorescence as demonstrated previously [7]. The method was validated by titrations using BAPTA-5N as competitive fluorophore chelator (Table 2). Apo S100A2-WT displayed affinity constants of log K_1=3.61±0.24 M^{-1} and log K_2=4.22±0.26 M^{-1}. However, pre-loading the Zn^{2+} sites resulted in a dramatic drop (~300-fold) in Ca^{2+} affinity of one EF-hand and a smaller drop (~3-fold) in affinity of the second EF-hand. The Ca^{2+}-binding constants for Zn^{2+} loaded S100A2-WT are log K_1=3.08±0.12 M^{-1} and log K_2=1.76±0.49 M^{-1} (Fig. 4, Table 2). The strong decrease in Ca^{2+}-affinity of S100A2 upon Zn^{2+} binding was rather unexpected since Zn^{2+} binding to other S100 proteins like S100B or S100A12 increases Ca^{2+}-affinity [23,24]. Since the intracellular Ca^{2+} concentration does not reach sufficiently high levels to bind to Ca^{2+} sites with such low affinity, these results

Table 2
Ca^{2+}-binding constants of S100A2 determined by competition with BAPTA-5N or intrinsic change in tyrosine fluorescence

	BAPTA-5N log affinity/M^{-1} [a]	BAPTA-5N log affinity/M^{-1} [b]	Tyr fluorescence log affinity/M^{-1} [a]	Tyr fluorescence log affinity/M^{-1} [a, c]
S100A2-WT	K_1=3.45±0.07	K_1=4.2±0.1	K_1=3.61±0.24	K_1=3.08±0.12
	K_2=4.06±0.12	K_2=3.7±0.6	K_2=4.22±0.26	K_2=1.76±0.49
		K_3=3.7±0.8		
		K_4=4.7±0.7		
S100A2–C2S	n.d.	n.d.	K_1=3.56±0.15	K_1=3.47±0.08
			K_2=4.26±0.17	K_2=3.73±0.09
S100A2–C21S	n.d.	n.d.	K_1=3.35±0.21	K_1=3.34±0.16
			K_2=4.50±0.17	K_2=1.43±0.18

[a] Fitting 2 identical sets of 2 Ca^{2+}-binding affinities.
[b] Fitting 4 different Ca^{2+}-binding affinities.
[c] In the presence of Zn^{2+}.

imply that Zn^{2+}-loaded S100A2 is not able to act as a Ca^{2+} sensor.

In order to map the Zn^{2+}-binding site that abolishes Ca^{2+} binding, the Ca^{2+} affinities of S100A2–C2S and S100A2–C21S in the absence and presence of Zn^{2+} were determined. In the absence of Zn^{2+}, both S100A2 variants displayed similar Ca^{2+} affinities like S100A2-WT (Table 2). Upon addition of Zn^{2+} to S100A2–C21S, which lacks the essential Cys21 residue of the designated Zn^{2+} site 1, the Ca^{2+} affinity decreased considerably (Table 2) like in S100A2-WT, i.e. Ca^{2+}-binding affinity is decreased regardless of the status of Zn^{2+} binding site 1. In contrast, mutation of Cys2 in S100A2–C2S almost restored the Ca^{2+} affinity in the presence of Zn^{2+} (Fig. 4B). S100A2–C2S still contains site 1 but lacks the essential Cys2 of site 2, i.e. a large decrease in Ca^{2+} affinity occurs only upon Zn^{2+} binding to site 2. These results suggest Zn^{2+} binding might render S100A2 inactive as Ca^{2+} sensor.

3.5. Stoichiometry of zinc binding

Fractions from size exclusion chromatography containing Zn^{2+}-bridged S100A2 were analyzed for the Zn^{2+} content. The fractions containing tetramer exhibited a content of 1.3 Zn^{2+} per S100A2 subunit, i.e. 5.2 Zn^{2+} per tetramer. Protein fractions eluting at higher volume corresponding to a smaller molecular mass had a Zn^{2+} content of 0.9 Zn^{2+} per S100A2 subunit. In addition we assessed the Zn^{2+} stoichiometry in UV monitored Zn^{2+} titrations of S100A2. The protein concentration was 30 μM, i.e. approximately 1000-fold higher than the apparent K_d for Zn^{2+} (25 ± 6 nM). Thus, virtually all Zn^{2+} ions present were bound by S100A2, which enables the stoichiometry of Zn^{2+} per S100A2 to be determined. Upon addition of Zn^{2+} to S100A2-WT an increase in UV absorption between 205 and 240 nm was observed. UV difference spectra revealed a maximum at 203 nm ($\varepsilon = 10{,}000\ M^{-1}\ cm^{-1}$) and shoulders at 208 and 221 nm (Fig. 5). No further spectral changes were observed after addition of 1.3 equivalents of Zn^{2+} per S100A2-WT subunit, implying saturation of the binding sites. The observed spectral changes arise from (sulfur → Zn^{2+}) ligand to metal charge transfer (LMCT) bands and show that Zn^{2+} is bound by cysteine residues. Comparison of the spectra with those from Zn^{2+}-S100A3 [37] show that the extinction coefficient of Zn^{2+}–S100A2-WT is about 5 times lower and that the LMCT bands are not as pronounced as in the case Zn^{2+}–S100A3. S100A3 binds 2 Zn^{2+} per subunit, coordinated by 7 cysteine residues [37]. The stoichiometry of 1.3 Zn^{2+} ions per S100A2 shows that the protein binds less than 2 Zn^{2+} ions per subunit, as proposed previously [6,7]. Furthermore, the lower extinction coefficient points towards coordination by fewer cysteine residues than in the case of S100A3. Since Since nitrogen → Zn^{2+} LMCT bands overlay partially with those of the CysS → Zn^{2+} LMCT bands, it is difficult to obtain a precise number of Cys thiols involved in coordination. The intensity of the bands accounts for one to two cysteine ligands for the first Zn^{2+} bound.

The course of the Zn^{2+} titration (Fig. 5) is characterized by a steep slope until a stoichiometry of one equivalent of Zn^{2+} per S100A2-WT subunit is reached. The slope decreases slightly as a further 0.3 equivalents Zn^{2+} are added and saturation is reached. The data fit well to the results obtained from size exclusion chromatography and the Zn^{2+} content of the fractions containing S100A2 tetramer. The stoichiometry of approximately 1.3 Zn^{2+} per subunit can be readily explained by a stoichiometry of 5 Zn^{2+} per S100A2 tetramer.

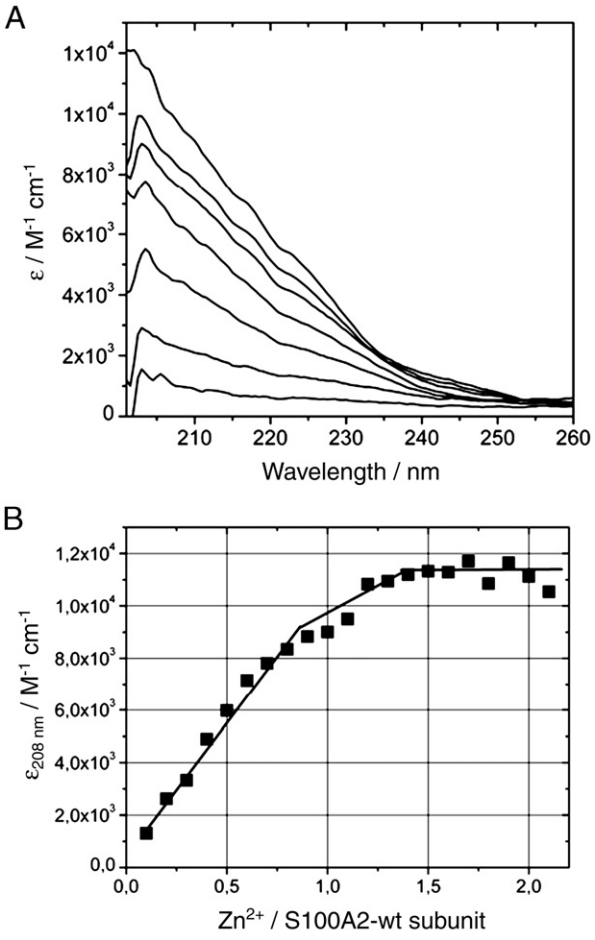

Fig. 5. Binding of Zn^{2+} to S100A2-WT monitored by UV difference spectroscopy. (A) Difference spectra of Zn^{2+} loaded S100A2-WT minus apo S100A2-WT. Protein concentration is 30 μM in 20 mM Tris–HCl, 5 mM $MgCl_2$, pH 7.6. Spectra for Zn^{2+} in the range 6–72 μM are shown. The extinction coefficient is calculated per S100A2 subunit. (B) Course of titration as monitored at 208 nm.

3.6. Zinc ligands and coordination geometry

The analysis of metal-binding sites by site directed mutagenesis is susceptible to misinterpretation in the case where mutation of some residues at distant sites have an unexpected long-range effect on the metal ion affinity [38,39]. Such effect may occur even though the coordination geometry is not directly affected. It is difficult to recognize such long range effects from affinity measurements. In order to discriminate between the elimination of a Zn^{2+}-binding site by mutation and long-range effects, we investigated the structure of the Zn^{2+}-binding sites in all S100A2 variants with Co^{2+} as an intrinsic spectroscopic probe and analyzed changes in metal ion coordination. Substitution of Zn^{2+} by Co^{2+} is a powerful tool,

which provides information on the nature of the ligands as well as on the geometry of the binding site. Representative UV/Vis, CD and MCD spectra of Co^{2+}–S100A2-WT and Co^{2+}–S100A2 variants are shown in Figs. 6 and 7. Octahedrally coordinated Co^{2+} usually shows weak d–d transitions in the visible region ($\varepsilon \approx 5–10\ M^{-1}\ cm^{-1}$) whereas the molar absorptivity increases up to 100-fold for tetrahedral coordination sites [40]. These electronic transitions at 500–800 nm are sensitive to the nature and number of ligand donor atoms. In the case of thiolate sulfur, the d–d absorption maxima shift towards lower energy and intense sulfur→Co^{2+} LMCT bands around 305–350 nm will appear.

Upon binding of Co^{2+} to S100A2-WT and its variants, distinct UV/Vis absorption maxima around 350 nm as well as between 500 and 700 nm (Figs. 6, 7) were observed. These features are absent in mutants where Cys21 was mutated to Ser (Fig. 7A, E). As a control, Zn^{2+} was added to Co^{2+}–S100A2. Displacement of the Co^{2+} was observed (data not shown), revealing that Co^{2+} binds specifically in the Zn^{2+}-binding sites. The intensity of the d–d transitions in the visible region with an ε of 300–500 $M^{-1}\ cm^{-1}$ is indicative of tetrahedral metal coordination. This conclusion is substantiated by the corresponding MCD spectra of Co^{2+}–S100A2-WT showing a strong MCD band at 665 nm, a shoulder at 606 nm and a weak positive band at 548 nm. Strikingly, the UV/Vis spectra of Co^{2+} substituted S100A2–C86S (Fig. 7B) and S100A2–C93S (Fig. 7C) closely resembles the spectrum of Co^{2+}–S100A2-WT (Fig. 6A) with identical maxima and extinction coefficients for the CysS→Co^{2+} as well as for the d–d transitions, demonstrating that no essential ligand was changed, neither in site 1 or in site 2.

Co^{2+}–S100A2–C2S, which lacks Cys2 required for Zn^{2+} site 2, shows a UV/Vis spectrum (Fig. 6D) similar to S100A2-WT with the maximum of the d–d transition shifted to 623 nm ($\varepsilon \approx 315\ M^{-1}\ cm^{-1}$). The MCD spectrum is slightly better resolved but reveals features similar to the spectrum of Co^{2+}–S100A2-WT with bands at 664 nm, a shoulder 617 nm, and a weak positive band at 563 nm. The CysS→Co^{2+} LMCT band around 350 nm in Co^{2+}–S100A2-C2S is not as well resolved as in Co^{2+}–S100A2-WT and its intensity is 40% lower demonstrating fewer CysS→Co^{2+} bonds. This observation is consistent with loss of site 2 in the C2S mutant.

The UV/Vis spectrum of Co^{2+}-substituted S100A2–C2S–C86S–C93S (Fig. 7D) is almost identical to that of Co^{2+}–S100A2–C2S. The overall intensity of the spectrum is somewhat lower, since fully saturated Co^{2+}–S100A2–C2S–C86S–C93S was not obtained due to protein precipitation. The optical data of Co^{2+}–S100A2C2S indicate that the remaining Zn^{2+} site 1 has tetrahedral geometry with a small distortion, and that this site only requires Cys21 as sulfur ligand. The position of the d–d transitions suggests that the three other ligands of Co^{2+} are nitrogen atoms, as coordination of Co^{2+} by one or two oxygen atoms would result in a shift towards shorter wavelength.

In contrast to the two C2S mutants, mutation of Cys21 results in the loss of resolved transitions in the d–d transition region of the UV-/Vis spectra of Co^{2+}–S100A2–C21S (Fig. 7A) and S100A2–C21S–C86S–C93S (Fig. 7E). This finding is explained by a distorted pseudo-tetrahedral coordination of Co^{2+} in site as shown by the lower extinction coefficient and the broad absorption envelope in the visible region. However, the difference spectrum between Co^{2+}–S100A2 WT and Co^{2+}–

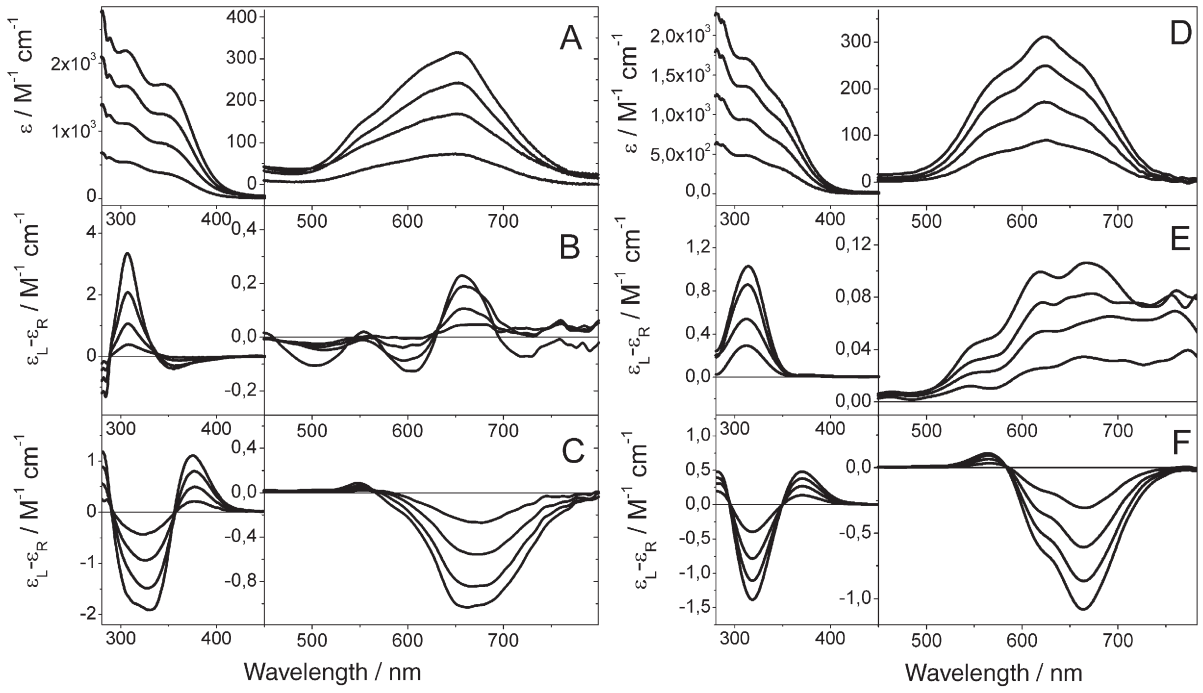

Fig. 6. Binding of Co^{2+} to S100A2 in 20 mM Tris–HCl, 5 mM $MgCl_2$, pH 8.3. (A–C) S100A2-WT 540 μM, Co^{2+} 135–540 μM,. The extinction coefficient is calculated per S100A2 subunit. (A) UV/Vis difference spectra, (B) CD spectra, (C) MCD spectra. (D–F) S100A2–C2S 600 μM with Co^{2+} in the range 150–600 μM. (D) UV/Vis difference spectra; (E) CD spectra; (F) MCD spectra. Addition of 1.3 equivalents Co^{2+} to S100A2-WT resulted in an overall increase in the intensity of the bands.

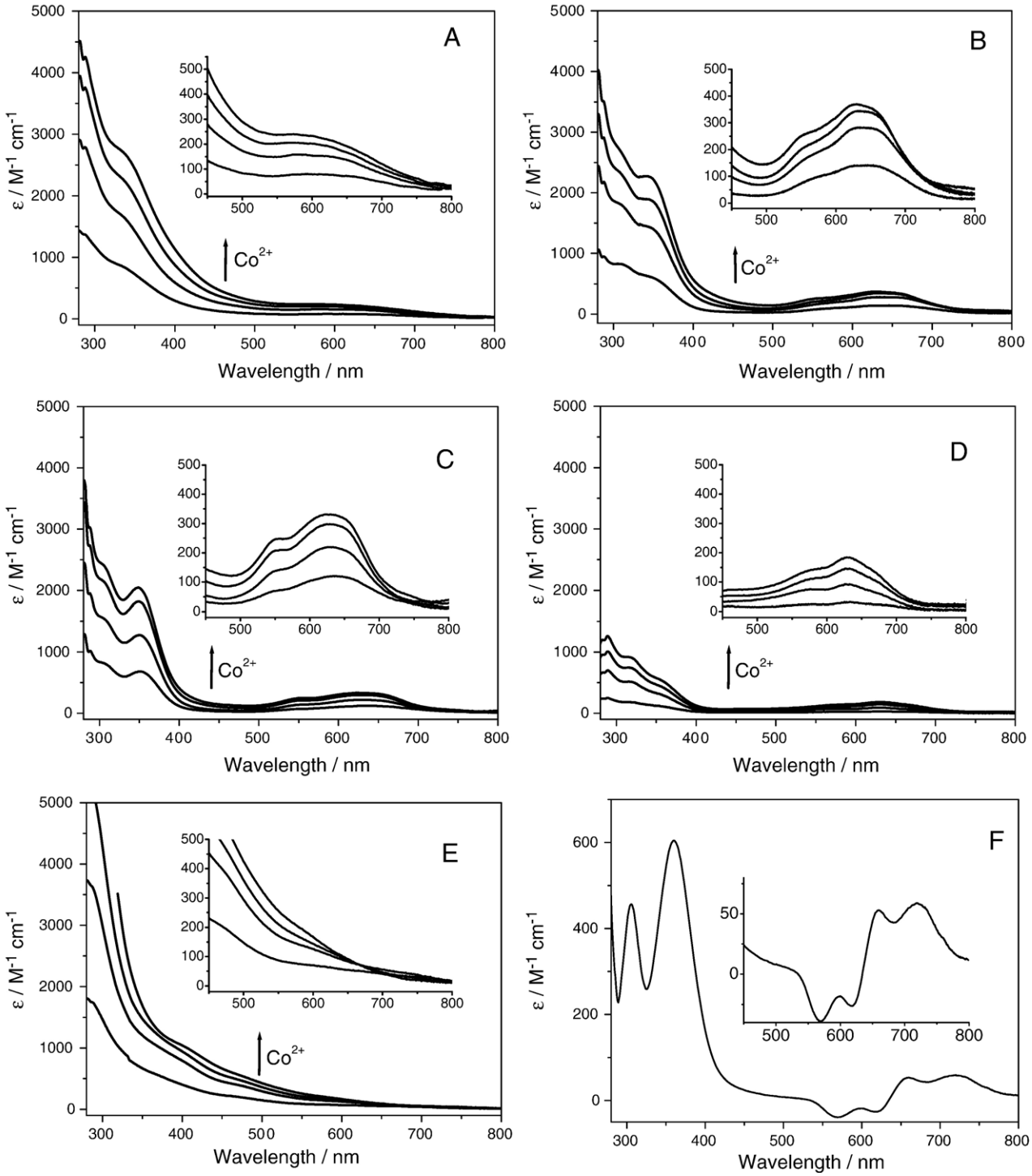

Fig. 7. Binding of Co^{2+} to S100A2 variants monitored by UV/Vis difference spectra. The buffer contains 20 mM Tris–HCl, 5 mM $MgCl_2$, pH 8.3. (A) S100A2–C21S 280 μM, Co^{2+} 280–1120 μM; (B) S100A2–C86S 270 μM, Co^{2+} 135–675 μM; (C) S100A2–C93S 275 μM, Co^{2+} 275–960 μM; (D) S100A2–C2S–C86S–C93S 260 μM, Co^{2+} 260–1170 μM; (E) S100A2–C21S–C86S–C93S 330 μM, Co^{2+} 330–1320 μM; (F) difference spectrum of Co^{2+}–S100A2–WT minus Co^{2+}–S100A2–C2S. The extinction coefficients are calculated per S100A2 subunit.

S100A2–C2S (Fig. 7F) which should give the spectrum of Co^{2+}-loaded site 2, shows well resolved features. These features were lost in the C21S mutants suggesting that mutation of site 1 influences the structure of site 2. The difference spectrum exhibits peaks at 305 and 360 nm in the UV region. The band centered at 360 nm ($\Delta\varepsilon = 600\ M^{-1}\ cm^{-1}$ per subunit, 2400 $M^{-1}\ cm^{-1}$ per tetramer) derives from additional $CysS \rightarrow Co^{2+}$ LMCT transitions in S100A2-WT. In the visible region two peaks at 660 nm and 720 nm ($\Delta\varepsilon = = 80\ M^{-1}\ cm^{-1}$ per subunit, 320 $M^{-1}\ cm^{-1}$ per tetramer) are observed corresponding to d–d transitions of site 2. A minor not well resolved shoulder is observed around 750 nm. The difference spectrum in the d–d

region closely resembles the spectra of Co^{2+}-loaded metallothioneins [41–43], which coordinate Co^{2+} with four Cys in a tetrahedral geometry and suggests that the Co^{2+} is coordinated mainly by cysteine residues.

The filling of Zn^{2+}-binding sites by Co^{2+} was followed to saturation, and the dissociation constants for Co^{2+} were calculated from a hyperbolic fit (Table 1). The values for the dissociation constants of the various Co^{2+}–S100A2 complexes correlate well with those determined for their corresponding Zn^{2+}–S100A2 counterparts. Although Co^{2+}-complexes have stability constants similar to those of Zn^{2+} complexes in the presence of oxygen donor atoms, differences in stability constants between Co^{2+} and Zn^{2+} complexes become pronounced for polarizable donor atoms such as nitrogen and sulfur [44]. The difference in affinity between Co^{2+} and Zn^{2+} has also been attributed to a loss in ligand field stabilization energy of the d^7 Co^{2+} ion as it changes from an octahedral hexa-aquo ion to a tetrahedral complex in the protein [45]. As expected the affinities for Co^{2+} are about 1000-fold lower, i.e. in the μM vs. nM range for Zn^{2+} (Table 1). The presence of high-spin Co(II) in a tetrahedral metal coordination was further supported by EPR spectroscopy which is not in contradiction with this coordination type (see Supplementary data).

3.7. Mapping of zinc induced structural changes by NMR spectroscopy

NMR spectroscopy was used to characterize the structural changes induced by the binding of Zn^{2+} to the wild-type protein. Addition of 0.9 molar equivalents of Zn^{2+} to the wild-type apo-S100A2 protein results in small chemical shift changes in the ^{15}N-^{1}H NMR spectrum. These perturbations were mapped to residues in the vicinity of the proposed Zn^{2+}-binding site 1 (Figs. 8, 9A, C). The absence of significant changes in the chemical shifts suggests there are only very limited conformational adjustments required for Zn^{2+} binding to the apo-protein. Addition of Zn^{2+} beyond one stoichiometric equivalent per subunit results in an increasing degree of broadening of the NMR signals and a significant loss in signal intensity. The latter observation is consistent with the formation of a higher molecular mass species, such as the tetramer observed by SEC and dynamic light scattering experiments.

3.8. 3D model of S100A2 and the metal binding sites

In order to characterize the structure of the binding sites, homology models of apo and Ca^{2+}-loaded S100A2 were constructed using the crystal structures of apo-S100A3 (pdb code 1KSO) [32], apo-S100A6 (pdb code 1K9P) and Ca^{2+}-loaded S100A6 (pdb code 1K96) [33] as templates. S100A2, S100A3 and S100A6 are closely related as indicated by sequence identities of 43% and 44%, respectively. The close relationship between S100A3 and S100A6 is documented by alignments of their 3D structures. The r.m.s.d of 1.03 Å over 164 Cα positions for the structures of the Ca^{2+}-free dimers reflects the great similarity of their tertiary structures. In view of the high level of sequence identity, it is reasonable to assume that S100A2 adopts the same tertiary structure as S100A3 and S100A6. The model of S100A2 comprises residues 1 to 94 but lacks the three C-terminal residues because the C-terminus of S100A3 was not resolved in the crystal structure and could not serve as a template. Both S100A6 and S100A3 bind Zn^{2+}. Each S100A6 subunit binds one Zn^{2+} at the N-terminus with Cys3 as one ligand (K_d=100 nM) [46], whereas S100A3 binds 2 Zn^{2+} per subunit with high affinity (apparent K_d=4 nM) [32]. The Zn^{2+} ions coordinate preferentially to thiolate sulfur (S_{Cys}) and imidazolyl nitrogen (N_{His}) as deduced from spectroscopic analyses [37].

A major question was whether the homology model would fit the spectroscopic data and whether it could be used to identify Zn^{2+} coordinating residues other than Cys21 and Cys2. Three out of four cysteine residues in the S100A2 model are

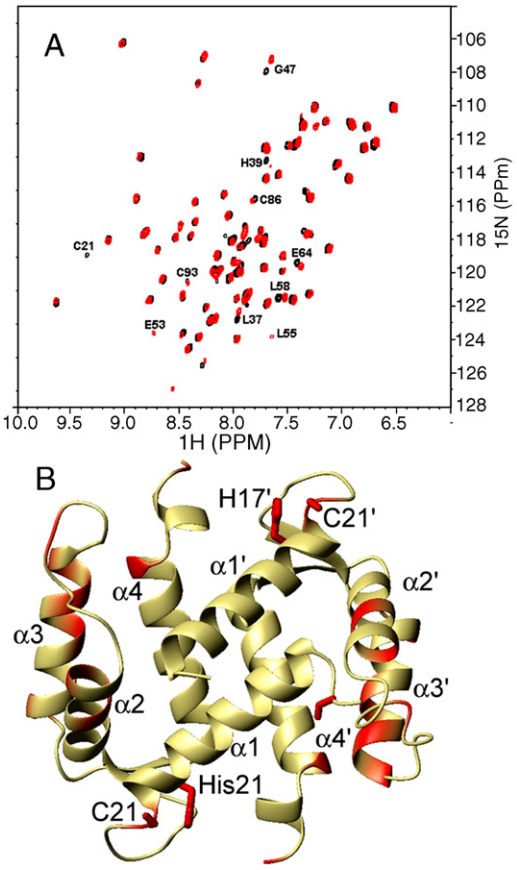

Fig. 8. Chemical shift mapping of S100A2-WT and S100A2-C2S Zn^{2+}-binding sites. (A) Overlay of ^{15}N–^{1}H HSQC spectra of 105 μM U–^{13}C,^{15}N labeled S100A2-WT in buffer containing 20 mM Tris–Cl, 90% H_2O/10% D_2O at pH 8.0 in the absence of Zn^{2+} ions (black contour lines) and with 0.9 equivalents of Zn^{2+} (red contour lines). Mapping of the Zn^{2+}-binding site based on chemical shift changes or intensity was complicated by the absence of assignments for apo-S100A2. Owing to differences in pH and buffer conditions, we were able to assign some but not all the resonances to specific residues based on previously published data [6]. (B) Homology model of apo-S100A2 color coded with assigned residues that showed a change in the weighted average of amide proton and nitrogen chemical shifts greater than 0.04 ppm (labeled in (A). All the NMR data were acquired on a 600 MHz Bruker AVANCE spectrometer at 27 °C. (For interpretation of the references to colour in this figure legend, the reader is referred to the web version of this article.)

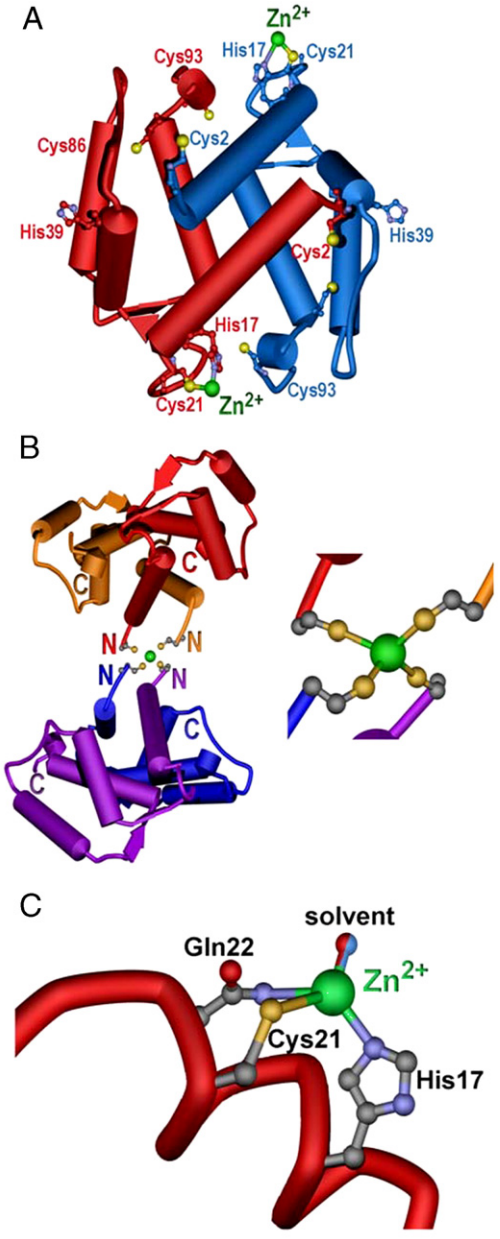

Fig. 9. Model of the three-dimensional structure of S100A2 and Zn^{2+} binding sites. (A) Zn^{2+}-binding site 1 at the homodimer interface. The two S100A2 subunits are shown in blue and red, and the Zn^{2+} ion in green. (B) Zn^{2+}-binding site 2 forming the S100A2 tetramer with the Zn^{2+} ion in green. (C) Putative structure of Zn^{2+}-binding site 1 including Gln22 in the coordination sphere; the fourth ligand is possibly a solvent molecule.

exposed to the solvent, i.e. Cys2 (63%), Cys21 (21%) and Cys93 (54%) (Fig. 9A). In contrast, the thiol group of Cys86 points inward towards the core and is surrounded by hydrophobic residues well shielded from the solvent (8% solvent accessibility). His17 resides one turn below Cys21 on helix I and the imidazole group is in the model close enough to the thiol of Cys21 so that they can coordinate the metal ion. The sidechain of His39 points to the solvent and the long distance from any other putative Zn^{2+} coordinating residue makes it is unlikely that His39 participates in Zn^{2+} binding. The involvement of the two C-terminal cysteine residues Cys86 and Cys93 in Zn^{2+} binding was proposed by previous studies [6–8]. However, the spectroscopic data of Co^{2+} substituted S100A2 and variants (Figs. 6, 7) rule out that Cys86 or Cys93 are ligands for Zn^{2+}. This is in agreement with the homology model where the sidechain of Cys86 is buried and Cys93 is located in the very C-terminus. Moving Cys93 into a Zn^{2+} coordinating position in site 1 would disrupt an array of conserved phenylalanine residues (Phe27′, Phe89, Phe90) which would be energetically quite unfavorable. In contrast Gln22 can coordinate Zn^{2+} in site 1 via its Nε nitrogen (Fig. 9C). A similar coordination of Zn^{2+} by a sidechain carboxamide has been observed in the crystal structure of a mutant of carboanhydrase II [47]. The spectra of Co^{2+}–S100A2 indicate that there is one sulfur and 3 nitrogen ligands in site 1. Such coordination is in agreement with coordination of Zn^{2+} by His17 and Gln22. However, there is no further residue in the proximity of Zn^{2+}-binding site 1 that could provide the putative third nitrogen for coordination. Nevertheless the site is located at the surface of the protein and the empty coordination site is solvent exposed (Fig. 9A C). Therefore the third nitrogen ligand detected in the Co^{2+} titrations might have been provided by a Tris molecule present in the buffer. Such a coordination by Tris has also been observed in a crystal structure of a mutant of carboanhydrase II [47]. In the absence of Tris a water molecule might serve as ligand.

Using size exclusion chromatography and dynamic light scattering, we showed that binding of Zn^{2+} to site 2 triggers the formation of a S100A2 tetramer. The spectroscopic data indicate that in the tetramer, one Zn^{2+} is coordinated by 4 cysteine residues, i.e. most likely each subunit provides Cys2 as ligand for the bridging Zn^{2+} (Fig. 9B). The model of apo-S100A2 reveals that the Cys2 residues from both subunits in the dimer have a distance of approximately 20 Å. This distance can decrease to 10 Å through a slight unwinding of helix I by only one residue combined with a movement of Ser3 and Ser4. Both serine residues following Cys2 are not involved in the dimer interface and do not form any sidechain hydrogen bonds in the model. Thus, it is conceivable that reorganization in the vicinity of the N-terminus could occur at low energy costs, which would be compensated by the contributions from binding of the Zn^{2+} ion. Such a scenario is supported by with the CD spectroscopic data, which show that Zn^{2+} binding to site 2 causes a slight decrease in α-helical content (Fig. 2).

4. Discussion

Our studies suggest that Zn^{2+} acts as a potent regulatory element for the nuclear EF-hand protein S100A2. Zn^{2+} binds to S100A2 with high affinity (apparent K_d 25±6 nM) and modulates the tertiary and quaternary structure as well as its affinity for Ca^{2+}. The availability of stable and well characterized Cys→Ser variants of S100A2 was essential, enabling assignment of the ligands within each of the Zn^{2+}-binding sites by various biophysical methods. We identified two Cys residues important for coordinating Zn^{2+}, Cys21 in site 1 and Cys2 in site 2.

Site 1 is located close to the dimer interface at the surface of S100A2. It is composed of the thiolate sulfur from Cys21 and

very likely by the imidazole nitrogen of His17 from one subunit. The optical and magnetic studies with Co^{2+} to probe site 1 reveal tetrahedral coordination, presumably with two further nitrogen ligands provided by Gln22 of the same subunit and a Tris molecule which could be replaced by another solvent molecule. Tetrahedral coordination of Zn^{2+}, as shown in our study by the Co^{2+} substitution experiments, was also observed in the structures of Zn^{2+}-loaded S100A7, S100A12 (Cu^{2+} in the Zn^{2+}-binding site) and S100B [48–50]. These three S100 proteins contain a common Zn^{2+}-binding motif: three out of four residues involved in metal ion coordination are conserved with regard to position and residue type: a His (S100A7, S100A12, S100B) and an Asp (S100A7, S100A12) or His (S100B) are located on the first subunit; a further His is contributed by the second subunit; the fourth ligand is a His or Glu from the second subunit. Interestingly, the first His of this well-conserved motif corresponds to His17 in S100A2. However, the Asp of this binding motif is replaced by a Phe in S100A2, which cannot coordinate Zn^{2+}. Cys21 compensates the missing Asp in S100A2 and thereby creates Zn^{2+}-binding site 1 which is different from other known S100 protein structures.

It is highly likely that Zn^{2+}-binding site 2 in S100A2 is formed by the association of two S100A2 homodimers, such that coordination of one Zn^{2+} ion is coordinated by the four Cys2 residues in a tetrahedral geometry [$Zn(Cys2)_4$]. Each dimer provides two Cys to coordinate the Zn^{2+}, triggering the formation of the observed tetramer. In an alternative model each S100A2 dimer might provide only one Cys2 residue which would result in a mixed coordination by sulfur, nitrogen/oxygen, however the data presented here are in better agreement with coordination by 4 Cys sulfurs. Furthermore the results from bis-ANS fluorescence experiments suggest that Zn^{2+} binding to site 2 induces the exposure of hydrophobic residues which might stabilize the protein–protein interaction. A similar dimerization of two entities triggered by a metal-ion bridging both proteins was observed in the structures of Zn^{2+}-bridged Rad50 [51] and the Cu^{+} linked ATX1–Ccc2 complex [52]. The driving forces for the protein complex formation were metal ion binding as we observe here for S100A2.

NMR data provides additional insight into the local environmental of the Zn^{2+}-binding site 1. The site is most likely preformed in the apo and Ca^{2+}-loaded states of S100A2 as indicated by the Ca^{2+}-binding and modeling data. Hence, introducing Zn^{2+} at this site has a minor effect on the overall secondary and tertiary structure of the protein as reported by NMR and other biophysical measurements. In contrast, structural changes were triggered by Zn^{2+} binding at site 2 as shown by CD spectroscopy.

Zn^{2+} is highly abundant in the cell where it is tightly bound to glutathione and Zn^{2+}-binding proteins. Consequently the concentration of free Zn^{2+} in a resting cell is assumed to be in the pM to low nM range. However, the intracellular Zn^{2+} concentration is not constant and rapid changes in free Zn^{2+} are observed in different cell types. Excitation of neuronal cells results in a fast and transient increase in intracellular Zn^{2+} of at least 40 nM [53]. In particular nuclear Zn^{2+} release was observed in injured neurons [54] and in endothelial cells upon activation of inducible NO synthase [55]. At such elevated concentrations, Zn^{2+} will bind to human S100A2 interrupting nuclear Ca^{2+} signaling pathways. Remarkably, the orthologous proteins from cow and dog lack the Cys2 and Cys21 residues, required for Zn^{2+} binding. This strongly implies that S100A2 in these organisms will not bind Zn^{2+} and suggests that the regulation of S100A2 by Zn^{2+} is specific for primates. The role of Zn^{2+} as a regulatory ion has been shown for intracellular signaling proteins, including protein tyrosine phosphatases [56] or caspases [57]. S100B [23,36,50] and S100A12 [58] have an affinity in the nM range for Zn^{2+} like S100A2. However, Zn^{2+} binding to S100B and S100A12 increases the Ca^{2+}-affinity (S100B ca. 3-fold; S100A12 ca. 1500 fold), whereas Zn^{2+} binding to S100A2 decreases its Ca^{2+} affinity (ca. 300-fold), underlining the role of Zn^{2+} binding as a regulatory element.

In contrast to the transient elevated concentrations of free intracellular Zn^{2+} noted above, prolonged increased Zn^{2+} concentrations are observed under oxidative stress conditions. Zn^{2+} is released from zinc-proteins, metallothioneins, or zinc-glutathione complexes by oxidation of the coordinating thiol groups [59,60]. Nevertheless, the Zn^{2+}-binding sites of S100A2, which also involve cysteines as ligands, might stay intact at conditions of low oxidative stress due to the nuclear localization of S100A2. In the nucleus the levels of reduced glutathione are three-fold higher than in the cytoplasm [61] which protect nuclear S100A2 from oxidation. Such was observed in a previous study where oxidation of S100A2 in the nucleus did not occur when cells were incubated with hydrogen peroxide concentrations below 1 mM [62], whereas intracellular metallothionein oxidation and subsequent Zn^{2+} release is observed already at 200 μM hydrogen peroxide [63]. We propose that the availability of free Zn^{2+} under conditions of oxidative stress may inhibit S100A2 mediated Ca^{2+} signaling, like e.g. p53 activation. Oxidative stress is a significant driving force in carcinogenesis [64] and Zn^{2+} released by extended low level oxidative stress might contribute to the carcinogenity by reducing the activation of p53 through S100A2. Further studies to characterize the influence of Zn^{2+} on the S100A2–p53 interaction are under way.

Acknowledgements

We thank Dr. H. Troxler for the MS analyses. This work was supported by Deutsche Forschungsgemeinschaft (Transregio-SFB 11, CH, GF, PK), Swiss National Science Foundation (grant 3100A0-111884/1, MV), Wilhelm-Sander-Stiftung, US National Institute of Health (grant RO1 GM62112, WJC) Vanderbilt Center in Molecular Toxicology (P30 ES000267, WJC), and Vanderbilt-Ingram Cancer Center (P50CA068485, WJC).

Appendix A. Supplementary data

Supplementary data associated with this article can be found, in the online version, at doi:10.1016/j.bbamcr.2006.12.006.

References

[1] G. Fritz, C.W. Heizmann, 3D structures of the calcium and zinc binding S100 proteins, in: A. Messerschmidt, W. Bode, M. Cygler (Eds.), Handbook of Metalloproteins, vol. 3, John Wiley and Sons, Inc., Chichester, 2004, pp. 529–540.

[2] C.W. Heizmann, G. Fritz, B.W. Schäfer, S100 proteins: structure, functions and pathology, Front. Biosci. 7 (2002) d1356–d1368.

[3] A. Mandinova, D. Atar, B.W. Schäfer, M. Spiess, U. Aebi, C.W. Heizmann, Distinct subcellular localization of calcium binding S100 proteins in human smooth muscle cells and their relocation in response to rises in intracellular calcium, J. Cell Sci. 111 (1998) 2043–2054.

[4] I. Marenholz, C.W. Heizmann, G. Fritz, S100 proteins in mouse and man: from evolution to function and pathology (including an update of the nomenclature), Biochem. Biophys. Res. Commun. 322 (2004) 1111–1122.

[5] A. Mueller, B.W. Schäfer, S. Ferrari, M. Weibel, M. Makek, M. Höchli, C. W. Heizmann, The calcium-binding protein S100A2 interacts with p53 and modulates its transcriptional activity, J. Biol. Chem. 280 (2005) 29186–29193.

[6] A. Randazzo, C. Acklin, B.W. Schäfer, C.W. Heizmann, W.J. Chazin, Structural insight into human Zn^{2+}-bound S100A2 from NMR and homology modeling, Biochem. Biophys. Res. Commun. 288 (2001) 462–467.

[7] T.B. Stradal, H. Troxler, C.W. Heizmann, M. Gimona, Mapping the zinc ligands of S100A2 by site-directed mutagenesis, J. Biol. Chem. 275 (2000) 13219–13227.

[8] C. Franz, I. Durussel, J.A. Cox, B.W. Schäfer, C.W. Heizmann, Binding of Ca^{2+} and Zn^{2+} to human nuclear S100A2 and mutant proteins, J. Biol. Chem. 273 (1998) 18826–18834.

[9] R.J. Cousins, J.P. Liuzzi, L.A. Lichten, Mammalian zinc transport, trafficking, and signals, J. Biol. Chem. 281 (2006) 24085–24089.

[10] B.L. Vallee, K.H. Falchuk, The biochemical basis of zinc physiology, Physiol. Rev. 73 (1993) 79–118.

[11] J.H. Laity, B.M. Lee, P.E. Wright, Zinc finger proteins: new insights into structural and functional diversity, Curr. Opin. Struct. Biol. 11 (2001) 39–46.

[12] M. Vasak, D.W. Hasler, Metallothioneins: new functional and structural insights, Curr. Opin. Chem. Biol. 4 (2000) 177–183.

[13] D.D. Perrin, A.E. Watt, Complex formation of zinc and cadmium with glutathione, Biochim. Biophys. Acta 230 (1971) 96–104.

[14] H. Haase, S. Hebel, G. Engelhardt, L. Rink, Flow cytometric measurement of labile zinc in peripheral blood mononuclear cells, Anal. Biochem. 352 (2006) 222–230.

[15] D. Atar, P.H. Backx, M.M. Appel, W.D. Gao, E. Marban, Excitation–transcription coupling mediated by zinc influx through voltage-dependent calcium channels, J. Biol. Chem. 270 (1995) 2473–2477.

[16] S.L. Sensi, L.M. Canzoniero, S.P. Yu, H.S. Ying, J.Y. Koh, G.A. Kerchner, D.W. Choi, Measurement of intracellular free zinc in living cortical neurons: routes of entry, J. Neurosci. 17 (1997) 9554–9564.

[17] L.M. Canzoniero, D.M. Turetsky, D.W. Choi, Measurement of intracellular free zinc concentrations accompanying zinc-induced neuronal death, J. Neurosci. 19 (1999) RC31.

[18] C. Frederickson, Imaging zinc: old and new tools, Sci. STKE 2003 (2003) pe18.

[19] J.M. Berg, Y. Shi, The galvanization of biology: a growing appreciation for the roles of zinc, Science 271 (1996) 1081–1085.

[20] R.J. Cousins, J.P. Liuzzi, L.A. Lichten, Mammalian zinc transport, trafficking, and signals, J. Biol. Chem. (in press).

[21] D. Beyersmann, H. Haase, Functions of zinc in signaling, proliferation and differentiation of mammalian cells, Biometals 14 (2001) 331–341.

[22] T.V. O'Halloran, Transition metals in control of gene expression, Science 261 (1993) 715–725.

[23] J. Baudier, N. Glasser, D. Gerard, Ions binding to S100 proteins. I. Calcium- and zinc-binding properties of bovine brain S100 αα, S100a (αβ), and S100b (ββ) protein: Zn^{2+} regulates Ca^{2+} binding on S100b protein, J. Biol. Chem. 261 (1986) 8192–8203.

[24] E.C. Dell'Angelica, C.H. Schleicher, J.A. Santome, Primary structure and binding properties of calgranulin C, a novel S100-like calcium-binding protein from pig granulocytes, J. Biol. Chem. 269 (1994) 28929–28936.

[25] T. Ostendorp, C.W. Heizmann, P.M. Kroneck, G. Fritz, Purification, crystallization and preliminary X-ray diffraction studies on human Ca^{2+}-binding protein S100B, Acta Crystallogr. F61 (2005) 673–675.

[26] A.O. Pedersen, J. Jacobsen, Reactivity of the thiol group in human and bovine albumin at pH 3–9, as measured by exchange with 2,2′-dithiodipyridine, Eur. J. Biochem. 106 (1980) 291–295.

[27] K.A. McCall, C.A. Fierke, Colorimetric and fluorimetric assays to quantitate micromolar concentrations of transition metals, Anal. Biochem. 284 (2000) 307–315.

[28] M. Huang, D. Krepkiy, W. Hu, D.H. Petering, Zn-, Cd-, and Pb-transcription factor IIIA: properties, DNA binding, and comparison with TFIIIA-finger 3 metal complexes, J. Inorg. Biochem. 98 (2004) 775–785.

[29] I. Andre, S. Linse, Measurement of Ca^{2+}-binding constants of proteins and presentation of the CaLigator software, Anal. Biochem. 305 (2002) 195–205.

[30] K. Nakanishi, N. Berova, R.W. Woody, Circular Dichroism: Principles and Applications, 2nd ed.John Wiley and Sons, Inc., Chichester, 2000.

[31] G. Böhm, R. Muhr, R. Jaenicke, Quantitative analysis of protein far UV circular dichroism spectra by neural networks, Protein Eng. 5 (1992) 191–195.

[32] G. Fritz, P.R. Mittl, M. Vasak, M.G. Grütter, C.W. Heizmann, The crystal structure of metal-free human EF-hand protein S100A3 at 1.7-A resolution, J. Biol. Chem. 277 (2002) 33092–33098.

[33] L.R. Otterbein, J. Kordowska, C. Witte-Hoffmann, C.L. Wang, R. Dominguez, Crystal structures of S100A6 in the Ca^{2+}-free and Ca^{2+}-bound states: the calcium sensor mechanism of S100 proteins revealed at atomic resolution, Structure 10 (2002) 557–567.

[34] A. Fiser, A. Sali, Modeller: generation and refinement of homology-based protein structure models, Methods Enzymol. 374 (2003) 461–491.

[35] T.A. Jones, J.Y. Zou, S.W. Cowan, Kjeldgaard, Improved methods for building protein models in electron density maps and the location of errors in these models, Acta Crystallogr. A47 (1991) 110–119.

[36] P.T. Wilder, D.M. Baldisseri, R. Udan, K.M. Vallely, D.J. Weber, Location of the Zn^{2+}-binding site on S100B as determined by NMR spectroscopy and site-directed mutagenesis, Biochemistry 42 (2003) 13410–13421.

[37] G. Fritz, C.W. Heizmann, P.M. Kroneck, Probing the structure of the human Ca^{2+}- and Zn^{2+}-binding protein S100A3: spectroscopic investigations of its transition metal ion complexes, and three-dimensional structural model, Biochim. Biophys. Acta 1448 (1998) 264–276.

[38] A. Ababou, R.A. Shenvi, J.R. Desjarlais, Long-range effects on calcium binding and conformational change in the N-domain of calmodulin, Biochemistry 40 (2001) 12719–12726.

[39] M.R. Nelson, E. Thulin, P.A. Fagan, S. Forsen, W.J. Chazin, The EF-hand domain: a globally cooperative structural unit, Protein Sci. 11 (2002) 198–205.

[40] Y. Shi, R.D. Beger, J.M. Berg, Metal binding properties of single amino acid deletion mutants of zinc finger peptides: studies using cobalt(II) as a spectroscopic probe, Biophys. J. 64 (1993) 749–753.

[41] P. Faller, M. Vasak, Distinct metal-thiolate clusters in the N-terminal domain of neuronal growth inhibitory factor, Biochemistry 36 (1997) 13341–13348.

[42] M. Vasak, J.H. Kagi, Metal thiolate clusters in cobalt(II)-metallothionein, Proc. Natl. Acad. Sci. U. S. A. 78 (1981) 6709–6713.

[43] G. Meloni, K. Zovo, J. Kazantseva, P. Palumaa, M. Vasak, Organization and assembly of metal-thiolate clusters in epithelium-specific metallothionein-4, J. Biol. Chem. 281 (2006) 14588–14595.

[44] W. Maret, B.L. Vallee, Cobalt as probe and label of proteins, Methods Enzymol. 226 (1993) 52–71.

[45] B.A. Krizek, D.L. Merkle, J.M. Berg, Ligand variation and metal ion binding specificity in zinc finger peptides, Inorg. Chem. 32 (1993) 937–940.

[46] J. Kordowska, W.F. Stafford, C.L. Wang, Ca^{2+} and Zn^{2+} bind to different sites and induce different conformational changes in human calcyclin, Eur. J. Biochem. 253 (1998) 57–66.

[47] C.A. Lesburg, C. Huang, D.W. Christianson, C.A. Fierke, Histidine→-carboxamide ligand substitutions in the zinc binding site of carbonic anhydrase II alter metal coordination geometry but retain catalytic activity, Biochemistry 36 (1997) 15780–15791.

[48] O.V. Moroz, A.A. Antson, S.J. Grist, N.J. Maitland, G.G. Dodson, K.S. Wilson, E. Lukanidin, I.B. Bronstein, Structure of the human S100A12–copper complex: implications for host–parasite defence, Acta Crystallogr. D59 (2003) 859–867.
[49] D.E. Brodersen, J. Nyborg, M. Kjeldgaard, Zinc-binding site of an S100 protein revealed. Two crystal structures of Ca^{2+}-bound human psoriasin (S100A7) in the Zn^{2+}-loaded and Zn^{2+}-free states, Biochemistry 38 (1999) 1695–1704.
[50] P.T. Wilder, K.M. Varney, M.B. Weiss, R.K. Gitti, D.J. Weber, Solution structure of zinc- and calcium-bound rat S100B as determined by nuclear magnetic resonance spectroscopy, Biochemistry 44 (2005) 5690–5702.
[51] K.P. Hopfner, L. Craig, G. Moncalian, R.A. Zinkel, T. Usui, B.A. Owen, A. Karcher, B. Henderson, J.L. Bodmer, C.T. McMurray, J.P. Carney, J.H. Petrini, J.A. Tainer, The Rad50 zinc-hook is a structure joining Mre11 complexes in DNA recombination and repair, Nature 418 (2002) 562–566.
[52] L. Banci, I. Bertini, F. Cantini, I.C. Felli, L. Gonnelli, N. Hadjiliadis, R. Pierattelli, A. Rosato, P. Voulgaris, The Atx1–Ccc2 complex is a metal-mediated protein–protein interaction, Nat. Chem. Biol. 2 (2006) 367–368.
[53] S.L. Sensi, L.M. Canzoniero, S.P. Yu, H.S. Ying, J.Y. Koh, G.A. Kerchner, D.W. Choi, Measurement of intracellular free zinc in living cortical neurons: routes of entry, J. Neurosci. 17 (1997) 9554–9564.
[54] C.J. Frederickson, S.C. Burdette, S.L. Sensi, J.H. Weiss, H.Z. Yin, R.V. Balaji, A.Q. Truong-Tran, E. Bedell, D.S. Prough, S.J. Lippard, Method for identifying neuronal cells suffering zinc toxicity by use of a novel fluorescent sensor, J. Neurosci. Methods 139 (2004) 79–89.
[55] D.U. Spahl, D. Berendji-Grun, C.V. Suschek, V. Kolb-Bachofen, K.D. Kroncke, Regulation of zinc homeostasis by inducible NO synthase-derived NO: nuclear metallothionein translocation and intranuclear Zn^{2+} release, Proc. Natl. Acad. Sci. U. S. A. 100 (2003) 13952–13957.
[56] H. Haase, W. Maret, Intracellular zinc fluctuations modulate protein tyrosine phosphatase activity in insulin/insulin-like growth factor-1 signaling, Exp. Cell Res. 291 (2003) 289–298.
[57] D.K. Perry, M.J. Smyth, H.R. Stennicke, G.S. Salvesen, P. Duriez, G.G. Poirier, Y.A. Hannun, Zinc is a potent inhibitor of the apoptotic protease, caspase-3. A novel target for zinc in the inhibition of apoptosis, J. Biol. Chem. 272 (1997) 18530–18533.
[58] E.C. Dell'Angelica, C.H. Schleicher, J.A. Santome, Primary structure and binding properties of calgranulin C, a novel S100-like calcium-binding protein from pig granulocytes, J. Biol. Chem. 269 (1994) 28929–28936.
[59] W. Maret, Metallothionein/disulfide interactions, oxidative stress, and the mobilization of cellular zinc, Neurochem. Int. 27 (1995) 111–117.
[60] B. Zhang, O. Georgiev, M. Hagmann, C. Gunes, M. Cramer, P. Faller, M. Vasak, W. Schaffner, Activity of metal-responsive transcription factor 1 by toxic heavy metals and H_2O_2 *in vitro* is modulated by metallothionein, Mol. Cell. Biol. 23 (2003) 8471–8485.
[61] G. Bellomo, M. Vairetti, L. Stivala, F. Mirabelli, P. Richelmi, S. Orrenius, Demonstration of nuclear compartmentalization of glutathione in hepatocytes, Proc. Natl. Acad. Sci. U. S. A. 89 (1992) 4412–4416.
[62] T. Zhang, T.L. Woods, J.T. Elder, Differential responses of S100A2 to oxidative stress and increased intracellular calcium in normal, immortalized, and malignant human keratinocytes, J. Invest. Dermatol. 119 (2002) 1196–1201.
[63] A.R. Quesada, R.W. Byrnes, S.O. Krezoski, D.H. Petering, Direct reaction of H_2O_2 with sulfhydryl groups in HL-60 cells: zinc-metallothionein and other sites, Arch. Biochem. Biophys. 334 (1996) 241–250.
[64] P. Kovacic, J.D. Jacintho, Mechanisms of carcinogenesis: focus on oxidative stress and electron transfer, Curr. Med. Chem. 8 (2001) 773–796.